Magnetic and elastic properties of YCo_5 and $LaCo_5$ under pressure

Daniela Koudela,[1] Ulrich Schwarz,[2] Helge Rosner,[2] Ulrich Burkhardt,[2] Axel Handstein,[1] Michael Hanfland,[3] Michael D. Kuz'min,[1] Ingo Opahle,[1] Klaus Koepernik,[1] K.-H. Müller,[1] and Manuel Richter[1]

[1]*Leibniz-Institut für Festkörper- und Werkstoffforschung, IFW Dresden, PF 270116, 01171 Dresden, Germany*

[2]*Max-Planck-Institut für Chemische Physik fester Stoffe, Nöthnitzer Straße 40, 01187 Dresden, Germany*

[3]*European Synchrotron Radiation Facility, Boîte Postale 220, 38043 Grenoble, France*

(Received 27 September 2007; published 11 January 2008)

High hydrostatic pressure destroys the strong ferromagnetism in YCo_5. The transformation proceeds in a stepwise fashion, as a first-order phase transition ($P_{crit}=18\pm2$ GPa), and is accompanied by an isomorphic (without change of symmetry) lattice collapse and a topological change of the Fermi surface. Accurate full-potential density-functional calculations enable us to ascribe these phenomena to a quasi-one-dimensional 3*d*-like band, whose top under ambient pressure is situated ~0.1 eV below the Fermi level. Lattice compression drives the top of the nondispersive band—and the associated peak in the majority density of states—upward in energy, until they reach the Fermi level and the system becomes unstable. A similar transition at a somewhat higher pressure (23 GPa) is predicted for the isomorphous compound $LaCo_5$.

DOI: 10.1103/PhysRevB.77.024411 PACS number(s): 71.20.Lp, 75.30.Kz, 75.50.Cc

I. INTRODUCTION

The intermetallic compound YCo_5 is a highly anisotropic strong ferromagnet. With an anisotropy field of about 18 T at the temperature of liquid He,[1] it can be made coercive, i.e., able to withstand demagnetization. In addition, it has a high Curie point of nearly 1000 K. In this sense, it is what is called a typical hard magnetic material, a close relation of the former champion in the league of permanent magnets, $SmCo_5$. On the other hand, YCo_5 is an archetypal strong ferromagnet, meaning that its majority 3*d* subband is fully occupied. Therefore, its magnetic moment is stable in relation to factors that might affect the electronic bands, such as, e.g., moderate pressure. All the more surprising was the recent announcement that YCo_5 loses its magnetic strength under hydrostatic pressure[2], even though this finding by itself should hardly come as a surprise. Indeed, there is an example of $ThCo_5$—a poor relation in the family of 1-5 ferromagnets—where the Co atoms on the 3*g* sites are in a low-spin state already under ambient pressure, the high-spin state being recovered in strong magnetic fields.[3] Theoretically, the transition of YCo_5 to a low-spin state under contraction was predicted eight years ago,[4] but no estimate of the threshold pressure was made then. Without such an estimate, the prediction remains incomplete, for it is generally known that under a high enough pressure any ferromagnet, no matter how hard and strong, will eventually become nonmagnetic.

Truly interesting is how the transition to the low-spin state happens. A first-order phase transition takes place in YCo_5, when both the magnetization and the volume of the sample diminish in a stepwise fashion at a certain critical pressure. This is a rather rare phenomenon—a first-order phase transition that preserves the symmetry of the crystalline lattice while reducing its volume. Usually, such an isomorphic lattice collapse is driven by a change in the chemical bonding (e.g., in Ce or in SmS). The transition in YCo_5, in contrast, has a magnetoelastic origin.[2] More peculiarly still, it is at the same time a Lifshitz or an electronic topological transition (ETT). This means that it is triggered by a change in the topology of the Fermi surface and proceeds without any change in the lattice symmetry. In general, Lifshitz transitions are not phase transitions of first nor even of second order, but rather "of order $2\frac{1}{2}$."[5] However, as pointed out by Lifshitz himself,[6] in exceptional cases ETTs may proceed as first-order phase transitions. Apparently, this prediction is realized in YCo_5.

Thus, the transition in YCo_5 is in many respects unique, and this work is a detailed theoretical and experimental study of the phenomenon (a preliminary account was published elsewhere[2]). The paper is structured as follows. The next section contains a description of the computational and experimental details. Subsequently, in Sec. III, the results of the density-functional theory (DFT) for YCo_5 are presented. These are followed by the data obtained in the high-pressure x-ray diffraction experiments, Sec. IV. After a discussion of the results for YCo_5 in Sec. V, a prediction of a similar transition in an isomorphous compound $LaCo_5$ is made in Sec. VI. Section VII then concludes the paper.

II. METHODS

A. Density-functional theory calculations

The calculations were performed by means of the full-potential local-orbital minimum-basis band structure code FPLO,[7] release 3. The program was run in the scalar-relativistic mode and, occasionally, the fixed-spin-moment option was used.[8] The local spin density approximation (LSDA) to the exchange and correlation potentials was taken in the form proposed by Perdew and Wang.[9]

The reciprocal space mesh contained at least $30\times30\times30$ points within the Brillouin zone (1456 **k** points within the irreducible wedge). It proved sufficient in all cases to use 1000 Fourier components for constructing the Ewald potential. Convergence tests[10] found the total energies computed with the above parameters to have a relative uncertainty of

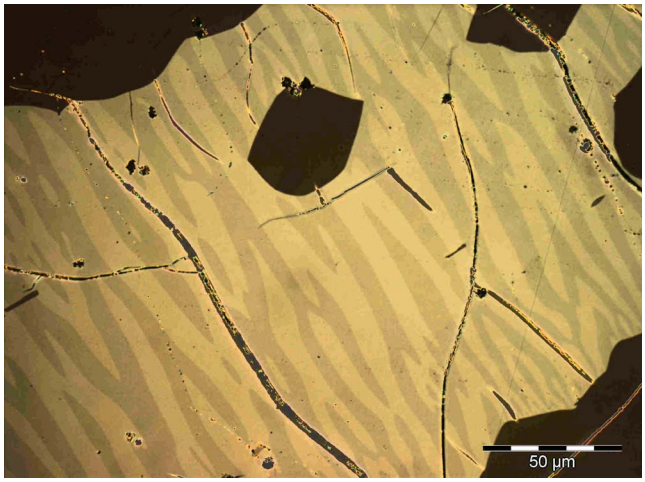

FIG. 1. (Color online) Homogeneous microstructure with YCo_5 grains of different orientations. Wavelike lamellae across the grains represent magnetic domains and can be influenced by external magnetic fields (polarized light image).

less than a few microhartrees per formula unit. The Co basis states used in our calculations were 3*sp* (semicore), 3*d*4*sp* (valence), and 4*d* (polarization). The Y basis comprised the 4*sp* semicore and the 4*d*5*sp* valence states. Addition of further polarization states (Co 4*f*, Y 4*f*, or 5*d*) produced no significant effect. The composition of the La basis was 5*sp* (semicore), 5*d*6*sp* (valence), and 4*f* (polarization).

YCo_5 has the hexagonal $CaCu_5$-type structure, space group $P6/mmm$, with Y occupying the 1*a* site and Co occupying the 2*c* and 3*g* sites. All the atoms are in special positions, therefore the lattice geometry is fully defined by the lattice constants, *a* and *c*. As the input values of *a* and *c* were varied, the aspect ratio was either kept constant ($c/a \equiv 0.81$, a value inferred from experimental data) or, alternatively, it was relaxed, i.e., determined by minimizing the total energy with respect to c/a at fixed volume. The minimum condition $[\partial E/\partial(c/a)]_V = 0$ follows from the relation $(\partial E/\partial a)_c = (2c/a) \times (\partial E/\partial c)_a$, which holds under hydrostatic pressure.[11]

B. Sample preparation

Polycrystalline YCo_5 samples were prepared by arc melting of elemental Y and Co in the nominal molar ratio 1:5 under a purified argon atmosphere. The purities of Y and Co were 99.9% and 99.95%, respectively. The YCo_5 button sealed in an Ar-filled quartz ampoule was homogenized by annealing at 1100 °C for seven days. The synthesized samples were characterized by metallographic methods, by chemical analysis, as well as by x-ray powder diffraction. Under polarized light, the optical microscopy of a polished sample reveals the presence of differently oriented grains (Fig. 1). The additional contrast within each grain is attributed to magnetic domains. Wavelength-dispersive x-ray spectroscopy measurements indicate an identical chemical composition of the differently oriented grains, with an average of 17.0(2) at. % Y and 82.7(2) at. % Co. This finding is within three standard deviations, in accordance with the target composition of 16.7 at. % Y and 83.3 at. % Co for YCo_5.

Chemical analysis of bulk samples detected no presence of hydrogen, nitrogen, or silicon (within the detection limits of 8, 20, and 50 ppm, respectively). The oxygen content was found to be 150 ppm, resulting in traces of diamagnetic Y_2O_3 as a contaminant phase. Additional 60 ppm Cu are due to the synthesis in a copper mold. Analysis for the main components by the optical emission of an inductively coupled plasma resulted in 22.0(1) wt % Y (as against 23.2 wt % calculated for YCo_5) and 76.6(2) wt % Co (76.8 wt% calculated).

The homogenized material was crushed in a hard-metal mortar and sieved for powder with a particle size of less than 60 μm. Then this powder was milled in a vibration ball mill for 40 min in toluene. The particle size after the milling was checked by scanning electron microscopy and found to be less than 20 μm. It can be assumed that most of the particles are single crystalline, due to grain growth during the prolonged homogenization. Such fine-grained powder is needed to ensure the presence of a sufficiently large number of randomly oriented grains in a small amount of material (restricted by the dimensions of the diamond culets with a diameter of 0.3 mm) in order to obtain the entirety of the Bragg reflections. To reduce residual mechanical stresses in the grains, the powder was annealed at 800 °C for 30 min in Ar. X-ray diffraction (Co $K\alpha$ radiation) of this powder revealed a nearly pure material of $CaCu_5$-type structure. In accordance with the findings of the chemical analysis, weak additional lines evidencing traces of Y_2O_3 were detected.

C. High-pressure experiments

Angle-dispersive x-ray powder diffraction data under hydrostatic pressures of up to 31 GPa were obtained using diamond anvil cells at the European Synchrotron Radiation Facility, Grenoble (ID09A, $\lambda = 41.75$ pm). In order to improve the powder average, the samples were rotated ±3° during the exposure. Helium was employed as a pressure-transmitting medium ensuring optimal hydrostatic or, at higher pressures, quasihydrostatic pressure conditions[12] even at low temperatures. Neon was used as an alternative medium for room-temperature measurements only. Cooling down to 100 K was achieved in a helium flow cryostat. Samarium-doped SrB_4O_7 was employed as a pressure sensor.[13,14] Two-dimensional diffraction images in the range $3° < 2\Theta < 25°$ were recorded by means of imaging plates, and the resulting diffraction data were azimuthally integrated with the computer program FIT2D.[15] The lattice parameters were refined by a least-squares procedure using full diffraction profiles.

III. YCo_5: DENSITY-FUNCTIONAL THEORY CALCULATIONS

A. Fixed-spin-moment calculations

The fixed-spin-moment (FSM) method, first proposed and implemented by Schwarz and Mohn,[8] is a standard technique for visualizing the presence of magnetically distinct states in a system. Our results for YCo_5 are presented in Fig. 2 as total energy versus spin magnetic moment curves, calculated at

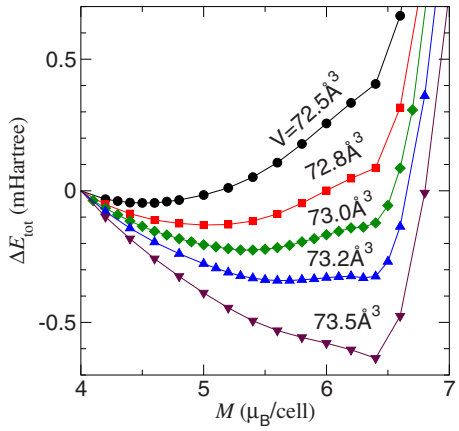

FIG. 2. (Color online) Calculated total energy versus spin magnetic moment curves for YCo_5. The total energy differences are normalized to zero at $M=4\mu_B$/cell.

several fixed volumes. The aspect ratio in all FSM calculations was kept constant, $c/a \equiv 0.81$.

The most important feature of Fig. 2 is the presence of curves with two minima within a narrow interval of volumes around $V=73.2$ Å^3. The right-hand minimum at $M \approx 6.4\mu_B$/cell corresponds to the high-spin (HS) state. This minimum disappears at lower volumes, as the HS state becomes unstable. The left-hand minimum, situated at $M \lesssim 5.5\mu_B$/cell, disappears at higher volumes, which indicates the instability of the low-spin (LS) state there. In the transition interval, both states coexist, one of them being stable and the other one metastable. Note that the terms HS and LS in this context refer to itinerant electronic states, not directly related to any particular atomic states of cobalt.

Our Fig. 2 is in qualitative agreement with Fig. 7 of Ref. 4. Quantitatively, the agreement is not as good, though. The respective features in Yamada's curves are shifted toward higher magnetic moments and higher volumes. Thus, their HS state has $M=6.8\mu_B$/cell, while ours has $M=6.4\mu_B$/cell; their critical volume is about 75.0 Å^3, as against our value, $V_{crit} \approx 73.2$ Å^3. The differences could be plausibly accounted for by the limitations of the earlier calculations.[4] First, it was the recourse to the atomic sphere approximation (ASA) in the linearized muffin-tin orbitals (LMTO) method and, second, the use of a different representation for the exchange and correlation potentials.[16]

B. Magnetic moment under pressure

The equilibrium values of the magnetic moment were obtained in the usual (non-FSM) self-consistent spin-polarized calculations. The results are plotted against volume in Fig. 3. The aspect ratio in these calculations was either fixed at $c/a=0.81$ (open squares) or relaxed, i.e., additionally optimized at each volume (filled circles). Also shown are the results of the earlier LMTO-ASA calculations,[4] carried out at the so-called ideal aspect ratio, $c/a \equiv \sqrt{2/3} \approx 0.816$. The slight deviations of the employed c/a were found not to be accountable for the difference between our results and those of Ref. 4.

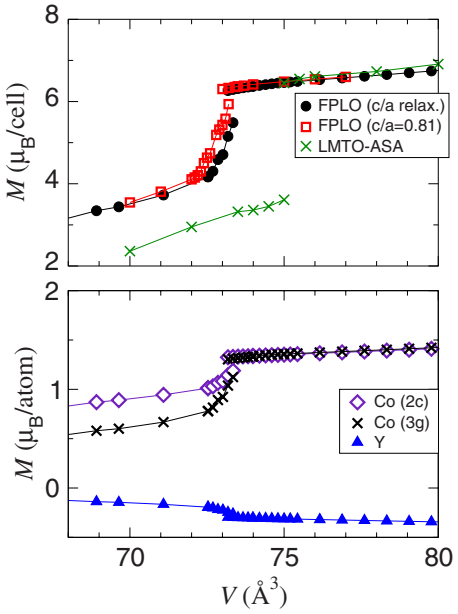

FIG. 3. (Color online) Upper panel: Magnetic moment per unit cell against volume. The open squares and filled circles refer to calculations performed with fixed and relaxed c/a, respectively. The asterisks are the LMTO-ASA calculations of Ref. 4. Lower panel: Calculated atomic magnetic moments against volume ($c/a=0.81$).

In the HS state, one observes a good agreement between all three sets of data points, the dependence of M on V being practically linear and very gently sloping. This is to be expected of a strongly ferromagnetic (saturated) HS state. Even the old LMTO-ASA calculations[4] fall in line here, unlike in the FSM case. It will be recalled that the HS minima in the FSM profiles of Ref. 4 were shifted to a higher value, $M \approx 6.8\mu_B$/cell. Now the self-consistent moment at the same volume is $M=6.5\mu_B$/cell (cf. Figs. 4 and 7 of Ref. 4). The discrepancy between the two values could be attributed to the use of the ASA and/or to basis incompleteness.

Turning now to the LS portions of the $M(V)$ curves in Fig. 3, we note a conspicuous difference between our results and those of Yamada *et al.*[4] Not only is the transition volume in Ref. 4 significantly higher, but the discontinuity is exaggerated as well. We find that on approach to the transition from the LS side, the moment experiences a rapid but continuous

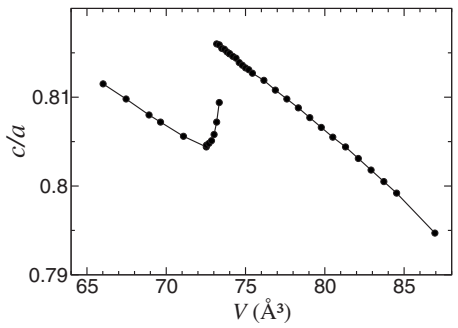

FIG. 4. Dependence of the relaxed c/a ratio on volume.

growth, until it finally undergoes a small abrupt change. The HS and LS branches do not merge. Rather, they coexist within a narrow interval of volumes. The region of rapid magnetization growth on the LS side of the transition is the only place where relaxing the c/a ratio produces a noticeable effect: it shifts the transition toward higher volumes and widens the discontinuity gap in the $M(V)$ curve.

The lower panel of Fig. 3 displays the behavior of the atomic magnetic moments. The Co atoms on two nonequivalent sites have the same moments in the HS state (where both are saturated), while in the LS state, the moment of Co($3g$) is significantly ($\sim 0.3\mu_B$) smaller than that of Co($2c$). The Y atoms carry a small negative moment roughly proportional to the total Co moment.

Stronger contraction makes the magnetization decrease further. The decrease on the LS side of the transition is continuous and extends down to $V \approx 57-58$ Å^3, where M finally vanishes. The threshold pressure of the transition to a nonmagnetic state is estimated at 100 ± 20 GPa.

C. Lattice parameters under pressure

As stated in Sec. II A above, hydrostatic conditions are truly reproduced when at each volume the total energy is a minimum with respect to c/a. These "relaxed" values of c/a were calculated and are plotted against V in Fig. 4. (The same values were employed in the previous section to compute the magnetic moment—filled circles in Fig. 3). The first-order transition point in Fig. 4 is manifested by a conspicuous "jump," superimposed on the otherwise gently sloping decrease of the aspect ratio with volume.

In real experimental conditions, pressure is fixed, rather than volume. In order to compute pressure, $P=-\partial E_{\text{tot}}/\partial V$, the total energy $E_{\text{tot}}(V)$ was taken at the relaxed c/a and fitted—the LS and HS branches separately—to seven different model equations of state.[17] To within line thickness, all seven yielded the same result, presented as V versus P in Fig. 5(a). In a certain range of pressures, the HS and LS phases can coexist. Such coexistence is characteristic of first-order transitions. Another remarkable feature in this figure is that the pressure calculated in the LSDA is shifted by about −15 GPa with respect to the "experimental" one. The latter is defined so as to vanish at the experimentally observed volume: $P_{\text{exp}}(V_{\text{exp}})=0$. However, $P_{\text{LSDA}}(V_{\text{exp}}) \approx -15$ GPa [see Fig. 5(a)].

The pressure dependence of the lattice parameters a and c [Figs. 5(b) and 5(c)] was computed from the data displayed in Figs. 4 and 5(a). One can observe a peculiarly anisotropic character of the volume collapse at the transition: the lattice shrinks abruptly, but only in one direction, along the sixfold axis. The dimensions in the basal plane vary almost continuously across the transition.

On account of the phase coexistence, it is not easy to locate the exact position of the transition point in the upper panels of Fig. 5. Rather, the threshold pressure can be found as the abscissa of the crossing point of the enthalpy curves $H(P)$ of the LS and HS states (it will be recalled that the enthalpy, $H=E_{\text{tot}}+VP$, is a characteristic thermodynamic function of pressure). To better visualize the crossing point in

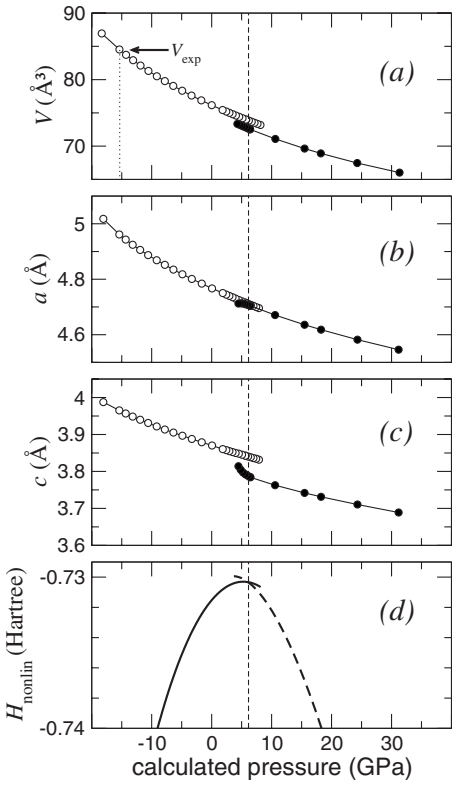

FIG. 5. (a) Unit cell volume and [(b) and (c)] lattice parameters versus calculated pressure. The arrow and the dotted vertical line in (a) indicate the experimental cell volume and the corresponding "experimental zero" on the pressure axis. (d) displays the pressure dependence of the nonlinear part of the enthalpy, $H_{\text{nonlin}}=H+[10337-P/(58.826\ \text{GPa})]$ hartree. The dashed vertical line marks the transition pressure, which is the abscissa of the crossing point of the two branches in (d), corresponding to the HS (solid) and LS (dashed) states.

Fig. 5(d), a common linear background, $[P/(58.826\ \text{GPa}) - 10337]$ hartree, was subtracted from both branches of the $H(P)$ dependence. This was to compensate for the steep growth of the two $H(P)$ curves. The so obtained transition pressure, ≈6 GPa on the LSDA pressure scale, is marked in all four panels of Fig. 5 with a vertical line. This value corresponds to about 21 GPa on the experimental pressure scale. The calculated volume jump is about 1.6%.

IV. PRESSURE EXPERIMENTS

X-ray powder diffraction patterns measured at various fixed pressures, reached both on rising and falling pressures, indicate that the hexagonal symmetry of the atomic arrangement remains unaltered within the investigated compression range (see Fig. 6). Least-squares refinements of the lattice parameters based on full diffraction profiles reveal a linear growth of the c/a ratio at $T=295$ K upon compression down to $V=77.9(1)$ Å^3, which corresponds to a pressure of 12.8(5) GPa (see Fig. 7). Further compression makes c/a drop momentarily, before resuming its growth at cell volumes below 74 Å^3 (pressures above 19 GPa). The singular

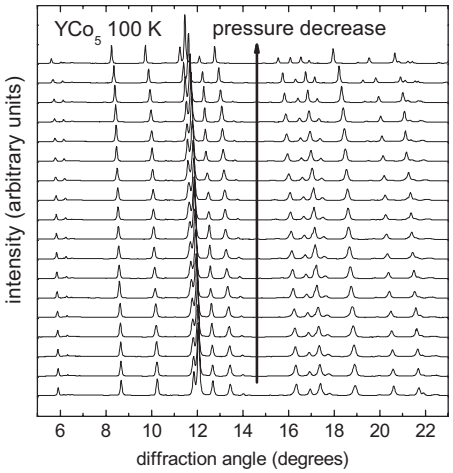

FIG. 6. X-ray powder diffraction patterns of YCo_5 at $T=100$ K and pressures between 1.3 and 30.6 GPa.

behavior is taken for an indication of an elastic anomaly in YCo_5.

Reduction of the temperature to 140 K sharpens the anomaly, shifting its onset to 76.2(2) Å^3, corresponding to 15.0(5) GPa. A yet more pronounced drop of c/a, amounting to as much as 0.6%, is observed at $T=100$ K (crosses in Figs. 7 and 8). The transition pressure is estimated as 18 ± 2 GPa. The temperature dependence of the transition can be ascribed to a reduction of the ordered magnetic moment at higher T.

The observed pressure dependence of the cell volume below the anomaly was fitted to a Murnaghan-type expression,[19] $V(P)=V_0(1+PB_0'/B_0)^{-1/B_0'}$, where B_0' was fixed at 4. At $T=295$ K, the fit yielded $V_0=84.38(7)$ Å^3 for the zero-pressure cell volume and $B_0=135(2)$ GPa for the bulk modulus. The obtained value of V_0 is in agreement with the average over the 19 x-ray crystallographic data sets compiled

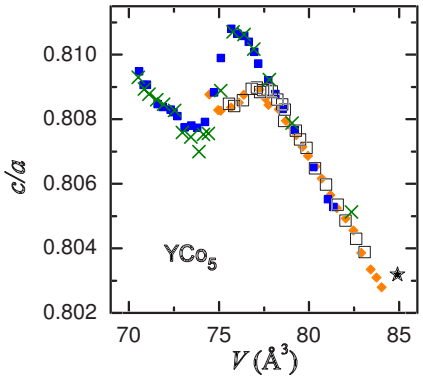

FIG. 7. (Color online) Aspect ratio c/a of YCo_5 as a function of unit cell volume, measured at three diffrerent temperatures. Orange diamonds ($T=295$ K) indicate the data obtained using neon as a pressure medium; open squares (295 K), filled blue squares (140 K), and green crosses (100 K) are the measurements with helium. The maximum compression corresponds to a pressure of 31.15 GPa. The asterisk marks the averaged ambient-pressure data from Ref. 18.

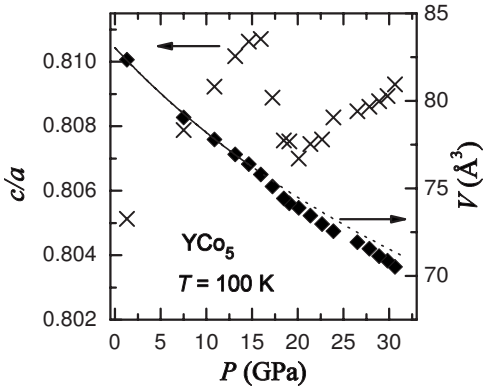

FIG. 8. Aspect ratio c/a (crosses) and unit cell volume (diamonds) of YCo_5 at 100 K plotted against pressure. A volume anomaly associated with the phase transition can be seen between about 16 and 20 GPa. Solid line: a fit of the experimental data below the phase transition to a Murnaghan-type expression. Dotted line: extrapolation of the fit into the stability range of the high-pressure phase.

in Ref. 18, $V_0=84.14(8)$ Å^3. Extrapolation of the Murnaghan dependence to higher pressures (dotted line in Fig. 8, $T=100$ K) yielded for the volume change associated with the transition a value of 0.9%.

V. DISCUSSION

YCo_5 has a peculiar band structure: there are two flat bands among its majority-spin subbands (Fig. 9). One of them has a two-dimensional character, with no visible dispersion in the direction of the sixfold symmetry axis, i.e., along the line ΓA. This band plays no major role in the pressure-induced first-order ETT in YCo_5. The other flat band is quasi-one-dimensional, with practically no dispersion in the basal plane (the triangle ΓKM). It is the latter band that will prove to be a key player in the first-order phase transition.

The two nondispersive bands are situated near the upper edge of the combined Co $3d$ majority subband. The quasi-one-dimensional band gives rise to a sharp peak in the majority (spin-up) density of states (Fig. 10). [The density of states (DOS) at the top of a truly one-dimensional band would diverge as $(E_{top}-E)^{-1/2}$]. The first-order Lifshitz tran-

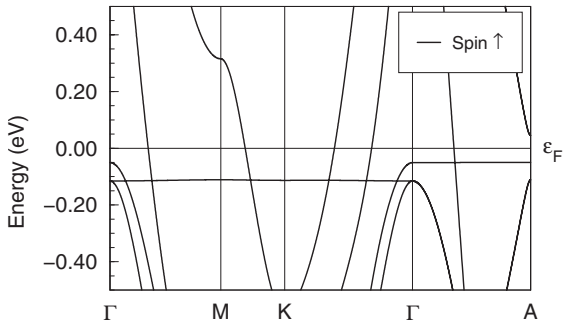

FIG. 9. Majority-spin part of the band structure of YCo_5 in a HS state ($V=76.16$ Å^3 and $c/a=0.812$).

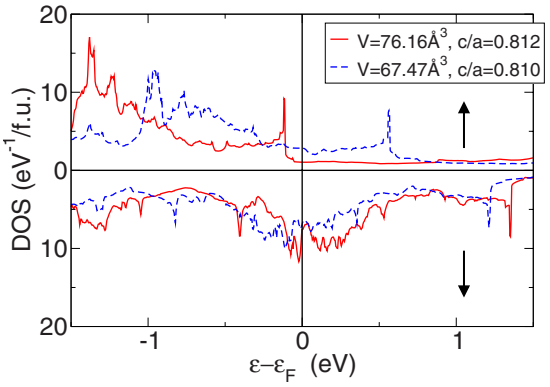

FIG. 10. (Color online) Total spin-polarized density of states of YCo_5. The red solid curve refers to a HS state, while the blue dashed one to a LS state.

sition in YCo_5 takes place when this peak crosses the Fermi level, cf. the red solid and blue dashed lines in Fig. 10, referring to the HS and LS states, respectively.

The situation when the peak is situated at the Fermi level is unstable. In this connection, note the always very high density of states at the Fermi level in the *minority* subband, $D_{\downarrow}(E_F)$ (Fig. 10). Now, when the narrow peak in the *majority* subband runs against the Fermi level, $D_{\uparrow}(E_F)$ becomes large as well as $D_{\downarrow}(E_F)$, so that Stoner's generalized stability condition,[20]

$$\frac{1}{4}\left[\frac{1}{D_{\uparrow}(E_F)}+\frac{1}{D_{\downarrow}(E_F)}\right] > I, \tag{1}$$

is no longer fulfilled. (Here, I is the Stoner parameter.) On account of the instability, the transition between the HS and LS states has to be discontinuous.

The two-dimensional band produces only a small steplike shoulder some 0.05 eV above the peak. This shoulder moves past the Fermi level in a continuous fashion (a usual ETT of order $2\frac{1}{2}$). Neglecting this shoulder, one can say that the $3d$ majority subband is fully occupied in the HS state (strong ferromagnetism, saturation of magnetic moment). In the LS state, the one-dimensional band is situated above the Fermi level and the combined $3d$ majority subband is partially depopulated (weak ferromagnetism).

The site-resolved densities of state (Fig. 11) provide evidence that only Co atoms contribute to the peak (note the much smaller scale in the left-hand panel). This contribution comes from the Co atoms situated on both nonequivalent sites in approximately equal proportion. Therefore, the peak heights for Co($2c\uparrow$) and Co($3g\uparrow$) are related as the respective site multiplicities, i.e., 2:3. It was earlier demonstrated (cf. Fig. 3 of Ref. 2) that the peak contains mainly $3d_{xz}$- and $3d_{yz}$-like states of Co. Interestingly, the little shoulder to the right of the peak is present in the right-hand panel of Fig. 11, but not in the middle one. The main constituent of the two-dimensional band is, therefore, the $3d$ states of Co($3g$).

VI. PREDICTIONS FOR $LaCo_5$

LSDA calculations were also performed for $LaCo_5$, which is isomorphous to YCo_5. A transition similar to that in YCo_5

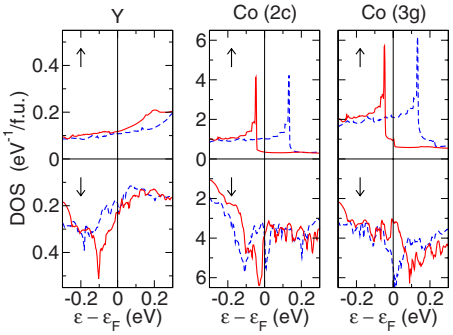

FIG. 11. (Color online) Site-resolved density of states near the Fermi level. The red solid line refers to a HS state just before the transition (V=74.0 Å^3 and c/a=0.81). The blue dashed line refers to a LS state directly after the transition (V=72.8 Å^3 and c/a =0.81).

was sought and found at cell volumes between 76 and 77 Å^3. Like in YCo_5, the lattice collapse in $LaCo_5$ proves extremely anisotropic: while the unit cell shrinks by about 1.2% along the sixfold symmetry axis, the cell dimensions in the basal plane show no discontinuity at the transition point (Fig. 12). The threshold pressure calculated in LSDA equals 7.7 GPa. For reasons explained in Sec. III C, this value needs to be corrected for overbinding. The correction (computed as the pressure at the experimental cell volume, ≈90 Å^3) turned out to be equal to 15 GPa, i.e., practically the same as in YCo_5. So we expect the transition in $LaCo_5$ to take place under a pressure of about 23 GPa.

VII. CONCLUSIONS

Our density-functional calculations show that hydrostatic pressure induces an electronic topological transition in the strong ferromagnet YCo_5. This transition is of first order and

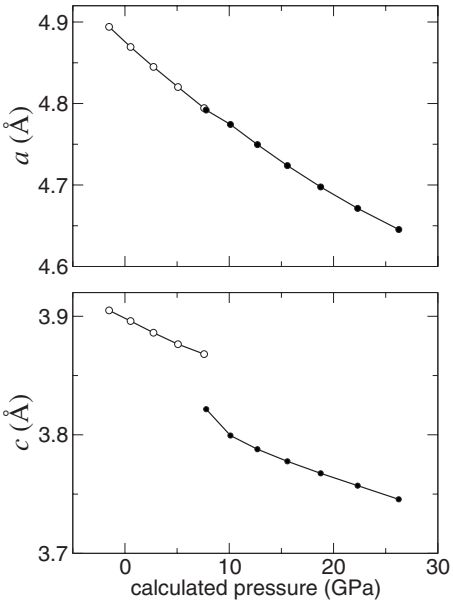

FIG. 12. Lattice parameters of $LaCo_5$ versus pressure calculated in LSDA. The open and closed circles refer to the HS and LS states, respectively.

is accompanied by a stepwise drop of the magnetic moment and by an isomorphic lattice collapse of a peculiar anisotropic kind. The unit cell shrinks abruptly in one direction only—along the sixfold symmetry axis—while its dimensions in the basal plane remain unchanged. The threshold pressure of the transition calculated in LSDA equals 6 GPa, which becomes 21 GPa upon correcting for the well-known overbinding of the LSDA.

Our high-pressure powder x-ray diffraction experiments on YCo_5 confirm these predictions. A first-order transition is observed at around 18 GPa and the measured aspect ratio c/a (Fig. 7) resembles the calculated one (Fig. 4). The measured volume drop amounts to -0.9%.

For the isostructural compound $LaCo_5$, calculations predict a similar transition at a slightly higher pressure.

The origin of the first-order ETT in YCo_5 and $LaCo_5$ lies in a quasi-one-dimensional band situated at ambient pressure just below the Fermi level. This band is composed primarily of Co 3*d* states, with approximately equal contributions from both nonequivalent Co sites, and forms the upper edge of the combined 3*d* majority-spin subband. Under pressure, this band first gradually shifts toward higher energies. When its top, associated with a sharp peak in the density of states, approaches the Fermi level, Stoner's generalized stability condition is violated, so the top of the band jumps over E_F. The band (as well as the entire majority 3*d* subband) suddenly becomes partially depopulated—a transition from strong to weak ferromagnetism. The one-dimensionality of the band, thus, appears responsible for the ETT being of first order.

ACKNOWLEDGMENTS

The authors are grateful to Viktor Yushankhai and John Mydosh for illuminating discussions and to Gudrun Auffermann, Anja Völzke, and Ulrike Schmidt for chemical analysis. Work at Dresden was financially supported by Deutsche Forschungsgemeinschaft (SFB 463 and Emmy-Noether-Program). The experiments at Grenoble were supported by the ESRF (Proposal No. HS-2379).

[1] J. M. Alameda, D. Givord, R. Lemaire, and Q. Lu, J. Appl. Phys. **52**, 2079 (1981).
[2] H. Rosner *et al.*, Nat. Phys. **2**, 469 (2006).
[3] D. Givord, J. Laforest, and R. Lemaire, J. Appl. Phys. **50**, 7489 (1979).
[4] H. Yamada, K. Terao, F. Ishikawa, M. Yamaguchi, H. Mitamura, and T. Goto, J. Phys.: Condens. Matter **11**, 483 (1999).
[5] Y. M. Blanter, M. I. Kaganov, A. V. Pantsulaya, and A. A. Varlamov, Phys. Rep. **245**, 159 (1994).
[6] I. M. Lifshitz, Sov. Phys. JETP **11**, 1130 (1960).
[7] K. Koepernik and H. Eschrig, Phys. Rev. B **59**, 1743 (1999); http://www.fplo.de
[8] K. Schwarz and P. Mohn, J. Phys. F: Met. Phys. **14**, L129 (1984).
[9] J. P. Perdew and Y. Wang, Phys. Rev. B **45**, 13244 (1992).
[10] D. Koudela, Ph.D. thesis, Technical University, Dresden, 2007.
[11] P. M. Marcus, F. Jona, and S. L. Qiu, Phys. Rev. B **66**, 064111 (2002).
[12] K. Takemura, J. Appl. Phys. **89**, 662 (2001).
[13] A. Lacam and C. Chateau, J. Appl. Phys. **66**, 366 (1989).
[14] F. Datchi, R. LeToullec, and P. Loubeyre, J. Appl. Phys. **81**, 3333 (1997).
[15] A. P. Hammersley, S. O. Svensson, M. Hanfland, A. N. Fitch, and D. Hausermann, High Press. Res. **14**, 235 (1996).
[16] U. von Barth and L. Hedin, J. Phys. C **5**, 1629 (1972).
[17] J. K. Dewhurst, EOS, Version 1.0, Program for fitting energy-volume data, 2002 (http://exciting.sourceforge.net).
[18] Pauling file binaries edition, Version 1.0, 2002.
[19] F. D. Murnaghan, Proc. Natl. Acad. Sci. U.S.A. **50**, 244 (1944).
[20] J. Kübler, *International Series of Monographs on Physics—Theory of Itinerant Electron Magnetism* (Oxford University Press, Oxford, 2000), Vol. 106.